33rd Annual International Conference of the IEEE EMBS
Boston, Massachusetts USA, August 30 - September 3, 2011

Scale-invariant Vesselness Filtering for Simultaneous Extraction of Optimal Medial and Boundary Paths in Retinal Images

Tao Zhu and Gerald Schaefer

Abstract—**In this paper we present a new multiscale vesselness filtering technique to simultaneously compute optimal medial axes and boundaries on fundus images of the retina. The scale-invariance of the vessel cross-sectional profile in the frequency domain is examined, and phase congruency implementing the scale-invariance is utilised for multiscale vesselness filtering. This allows the vessel ridge and boundary evidence to be preserved under single filtering settings. We have performed width measurement experiments on a dataset of fundus images, using an optimal medial axis skeletonisation scheme as a post-processing step, to compare the proposed technique with a generalised Gaussian profile modelling approach.**

I. Introduction

THERE are a variety of significant diseases (e.g., hypertension and diabetes) that affect blood vessels of the retina. Measurement of vessel geometry such as diameters, branching angles, and branching lengths, can play a valuable role in the study and diagnosis of these diseases [1]. For example, the change in width of vessels within the fundus is believed to be indicative of abnormalities in disease states [1]. Manual delineation of the vasculature structure in retinal fundus images is tedious and expensive. Thus, tools of vessel detections are sought to preserve measurement information. Automated tools have the potential to improve the reliability and repeatability of many forms of retinal examination while reducing the costs involved.

Frangi's vesselness filtering (or multiscale ridge detection) and its variants are popular for detection of blood vessels in angiography images [2] [3]. Generally, the optimal scale was chosen such that maximal vesselness response for individual pixels is obtained. These techniques however are unreliable to produce boundary evidence, since "vesselness" was used, based on the eigenvalue analysis of the Hessian intensity matrix in scale space, as an image feature. Some extensions have been reported incorporating boundary identification or pixel classification algorithms [4].

Sofka *et al.* used Gaussian matched filters in scale space to detect retinal vessel medials, and used edge measures to affect the confidence of medial nodes [5]. However, no optimal medials were produced, since the shape of the vessel was not taken into account. Wink *et al.* utilised Dijkstra's algorithm to find optimal medials and the corresponding scale values based on vesselness [6]. Their work was extended by incorporating vessel boundary evidence and the shape of the vessel [7]. Interestingly, several edge detectors were used jointly for estimating vessel boundary positions. The gradient magnitude filter was chosen to detect weak vessel edges, while Canny and Laplacian of Gaussian operators were less sensitive to noise. It is however difficult to determine appropriate threshold values on the response of vessel boundary to gradient-based edge detector, largely due to variations in contrast across retinal images.

In the rest of this paper, the scale-invariance of the vessel cross-sectional profile in the frequency domain is examined, and phase congruency implementing the scale-invariance is utilised for multiscale vesselness filtering. The performance of the algorithm is compared to that of some other commonly known algorithms.

II. Methodology

A. Vesselness in the Frequency Domain

In previous work, rectangular, Gaussian, and difference-of-dual Gaussian functions were often used to characterise vessel cross-sectional profiles extracted from retinal images. Let us examine the Fourier transforms of these three functions. We can readily see that the middle points (medial nodes) of these functions are indicated by the local extreme (maximum or minimum) magnitudes in the frequency domain respectively, while the middle point of a rectangular function cannot be identified from its local intensity information. More interestingly, the Fourier phases localised at their middle points are piecewise constant, where the two constant values are zero and π. It is therefore a natural choice to use phase information to determine the ridge of vessels.

Specifically, the Fourier series expansion of $f(x)$ is $f(x) = \sum_n A_n \cos(\phi_n(x))$ where ϕ_n is the phase offset of the *n*-th component of the expansion, and A_n is the amplitude. Consider that the phase is zero or π for all frequency components contained within it. We define a measure of vesselness as follows:

$$V\{f(x)\} = \frac{\sum_n \lfloor A_n(x)(\cos(\phi_n(x) - \phi_s)) \rfloor}{\sum_n A_n(x)} \qquad (1)$$

where ϕ_s is piecewise constant ($\phi_s = 0$ or π) at the point (x) being considered. The symbol $\lfloor \cdot \rfloor$ denotes that the enclosed quantity is equal to itself when its value is positive, and zero otherwise. This function gives a normalised

T. Zhu and G. Schaefer are with the Department of Computer Science, Loughborough University, Loughborough, U.K.

measure of vesselness, so as to be invariant to the magnitude of the signal $f(x)$. Also, it can be viewed as calculating the alignment degree of the phases of all frequency components with ϕ_s, $\phi_s = 0$ for a downward signal and $\phi_s = \pi$ for upward. In the presence of central light reflection, a cross-sectional profile still has a real even transform, and local high alignment degree is expected to remain unchanged.

B. Scale Invariance of Vessel Cross-Sectional Profile

A common method for extracting amplitude and phase data of a signal is via wavelets by convolving the signal with a quadrature pair of filters, e.g. log-Gabor filters in symmetric and anti-symmetric pairs. Let us review how the phase of a one-dimensional (1-D) signal evolves across scales in the wavelet domain. The wavelets constitute a family of functions derived from a *mother* wavelet by dilations and translations

$$w_{s,p}(x) = \frac{1}{\sqrt{s}} w\left(\frac{x-p}{s}\right) = \frac{1}{\sqrt{s}} g\left(\frac{x-p}{s}\right) e^{j\omega_c (x-p)/s}$$

where $s \in R^+$ is a scale factor, $p \in R$ is a translation factor, and $w(x)$ is a mother wavelet. The mother wavelet may be written as a modulation of a low-pass filter $g(x)$: $w(x) = g(x)e^{j\omega_c x}$, where ω_c is the centre frequency of the modulated band-pass filter, and $g(x)$ is a slowly varying and symmetric function. Given a real 1-D signal $f(x)$, the wavelet transform of the signal can be written as

$$F(s,p) = \left[f(x) \bullet \frac{1}{\sqrt{s}} g\left(\frac{x}{s}\right) e^{j\omega_c x/s} \right]_{x=p}$$

$$= \frac{1}{2\pi} \int_{-\infty}^{\infty} F(\omega) \sqrt{s} G(s\omega - \omega_c) e^{j\omega p} d\omega \qquad (2)$$

where $F(\omega)$ and $G(\omega)$ are the Fourier transforms of $f(x)$ and $g(x)$ respectively. Assuming that the signal $f(x)$ being analysed is localised near the position x_0, we rewrite the signal into a function $f_0(x)$ that satisfies $f(x) = f_0(x - x_0)$. Using Fourier shifting and scaling properties, we can rewrite (2) as

$$F(s,p) = \frac{1}{2\pi\sqrt{s}} \int_{-\infty}^{\infty} F_0\left(\frac{\omega}{s}\right) G(\omega - \omega_c) e^{j\omega(p-x_0)/s} d\omega \qquad (3)$$

where $F_0(\omega)$ is the Fourier transform of $f_0(x)$. If $F_0(\omega)$ is scale-invariant at x_0, we have

$$F_0\left(\frac{\omega}{s}\right) = K(s) F_0(\omega) \qquad (4)$$

where $K(s)$ is a real function of only s s, and is independent of ω. Combining (2) and (3), we obtain

$$F(s, x_0) = \frac{K(s)}{\sqrt{s}} F(1,p)\Big|_{p=x_0}$$

The phase can then be expressed as

$$\Phi(F(s, x_0)) = \pm\Phi(F(1, x_0)) \qquad (5)$$

Our analysis shows that the phases of all Fourier components contained in the signal $f(x)$ are aligned at x_0 if $F_0(\omega)$ is scale-invariant.

Recall that the distribution is modelled as rectangular, Gaussian, or difference-of-dual Gaussians. Apparently the Fourier transform of any profile satisfies (4) having the scale-invariant property. This allows vesselness to be measured by assessing phase alignment with zero or π. However, it is necessary to preserve vessel boundary evidence. Consider that the Fourier transform of a Heaviside step function satisfies (4). The corresponding phase at the half height (i.e., the vessel boundary) is expected to be aligned with $\pm\pi/2$.

C. Implementation of Scale-invariant Vessel Filtering

The Kovesi phase congruency model of feature detection is a computationally efficient implementation of defining phase congruency on 2-D images, and incorporated by a simple and adaptive noise resistance algorithm [8]. We utilise the Kovesi phase congruency function $PC(x)$ to calculate phase alignment degree on 2-D images. Specifically, vesselness at x is measured by

$$M_v(x) = PC(x, \phi_v) \qquad (6)$$

where $\phi_v = \pi$ for upward profile curve, and $\phi_v = 0$ for downward. Similarly, vessel boundary is measured by

$$M_b(x) = PC(x, \phi_b) \qquad (7)$$

where $\phi_b = \pi/2$ for a rising boundary; and $\phi_b = -\pi/2$ for a falling boundary.

In scale space, the number of features reduces as the filter scale increases. It is necessary to choose appropriate filtering scales which are large enough to detect the vessel boundary, and small enough to avoid the merging of pairs of boundaries. Even if in a scale two boundaries start merging (the phases of the boundaries start drifting towards each other), local symmetry between the boundaries is expected to retain. Provided that the scale of filter is reasonable for boundary detection, localisation of vesselness is preserved.

The filter parameters of log-Gabor filters used in the Kovesi phase congruency model have been experimentally set with respect to the significance of composite features including step and ramp changes. Since a half-height feature is around the centre of a step or a ramp, it is reasonable to start from the filter settings as in [8] [9]. The feature significance functions (6) and (7) are applied on data from oriented 2-D log-Gabor wavelets. In our experience, we have found that six orientations with four resolution levels (scales) increasing the wavelength by 0.2 octaves, provided a good compromise between computational expense and accuracy of experimental results.

D. Extraction of Optimal Medial and Boundary Paths

We adopted the optimal medial axis skeletonisation scheme as in [7] to simultaneously extract medials and boundary points of vessels with radii down to half pixel. In the medial axis skeletonisation scheme, the medial path of a

vessel is defined as the set of centres (medial nodes) of the maximal inscribed circles inside the vessel, denoted as the optimal spatial coordinates (x, y) and radius values r between two-sided boundary in 3-D space (x, y, r). The optimisation is achieved by minimising a cumulative cost function at each node, which describes the cost from node $q = (x, y, r)$ to a neighbouring node $p = (x', y', r')$.

To adapt the above scheme, we replaced its ridge detection and edge detection components with the measures of vesselness and vessel boundary, respectively. The cost function that describes the cost from node $q = (x, y, r)$ to a neighbouring node $p = (x', y', r')$ is defined by:

$$\text{cost}(q, p) = W_1 C_{ridge}(p) + W_2 C_{\Phi}(q, p) + W_3 C_{edge}(p) \quad (8)$$

where C_{ridge} corresponds to the measure of vesselness (5); C_{Φ} refers to the vessel direction change between q and p; and C_{edge} is a measure of the fitness of a medial node by assessing the boundary evidence of equidistant positions on either side. Each cost term is a normalised quantity with values in [0; 1]. For our experiments, we set the coefficients W_1, W_2, and W_3 to 1.0.

III. Experimental Results

A cropped original colour fundus image for illustrative purpose is given in Fig. 1(a), and the results of measuring asymmetry and symmetry are given in Figs. 1(b) and 1(c) respectively. The central light reflex is obvious on some vessel segments in the original image. The green component of the colour image was used only since this component provides the highest object contrast. From the results we readily observe that high asymmetry and symmetry of local Fourier components highlight the boundary and the inner part of the vessel segments, respectively. The response of the measure of asymmetry on two-sided boundary appears to be invariant to the presence of the central light reflex. Indeed, high asymmetry is also found on the effect of spurious noise. For the purpose of comparison, a Sobel operator was applied to the same image, and the corresponding filtered image is given in Fig. 1(d). Clearly, the response of the operator on two-sided boundary varies considerably, making it difficult to predefine appropriate threshold values for vessel edge detection. This problem is common to edge detectors based on differential operators. Comparing the filtered image with the asymmetry image, we may conclude that the proposed algorithm achieves significant improvement compared to other edge-based algorithms in alleviating the central light reflex problem.

Also, we performed a width measurement study on the results obtained from the ARIA dataset to illustrate the performance of the proposed algorithm. A total of 191 segments inside a ring-shaped zone with 70 pixels in diameter (see Zone B in Fig. 2) were selected from different images of the dataset. Given a pixel of a selected segment, we were able to extract a cross-section normal to the vessel axis (medial path), and compute an optimal vessel radius (or width) value. For the purpose of comparison, we implemented the HHFW (half-height-full-width) method, and the generalised Gaussian profile modelling as used in [10] and [11], to compute estimated width values on the extracted cross-section. Fitting the generalised model of two-Gaussians to a cross-section of intensities was performed by means of the Levenberg-Merquardt least squares method, to obtain a set of model parameters characterizing the vessel. Then the vessel width value was estimated to be equal to 3.26σ of the best fit. The median of five width values estimated for a selected pixel was taken to exclude outliers.

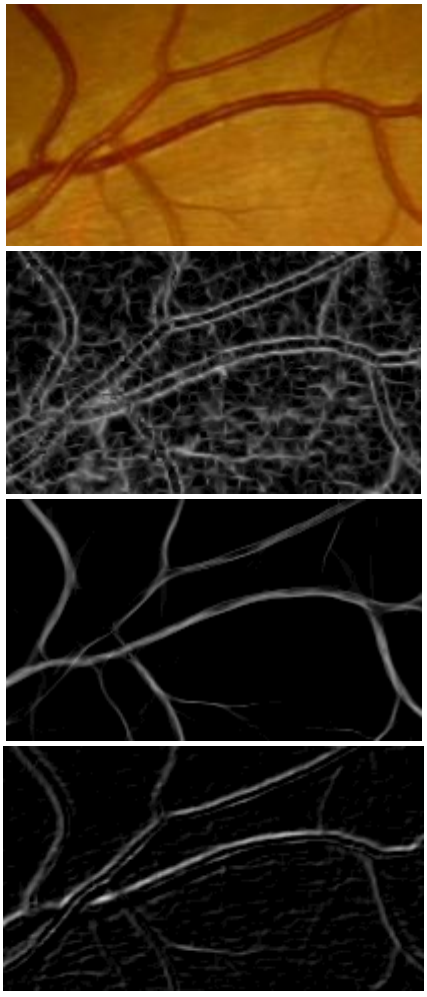

Fig. 1. Results of measuring asymmetry and symmetry on a colour fundus image: (a) the original image; (b) asymmetry image; (c) symmetry image; and (d) edge detection by using Sobel operator. The value at each location of the asymmetry and symmetry images is in the range [0, 1].

On all segments, the width estimates produced by the methods were recorded and used in subsequent analysis. Quantitative agreement between our width measurements and the HHFW values and between the generalised profile modelling measurements and the HHFW values respectively, is illustrated as a Bland-Altman plot in Fig. 3,

allowing the degree of variation present to be objectively analysed. Note that on 43 cases the experimental results produced by the generalised profile modelling were not recorded in Fig. 2(b) since finding the best fit was difficult, particularly on thin vessels. We can see that in comparison with the HHFW values, the width estimates computed using the detection method in the enhanced form show less scatter than those using the generalised profile modelling. Systematic differences appear between the set of HHFW values and the set of our measurements implying the comparability of the HHFW and our algorithm.

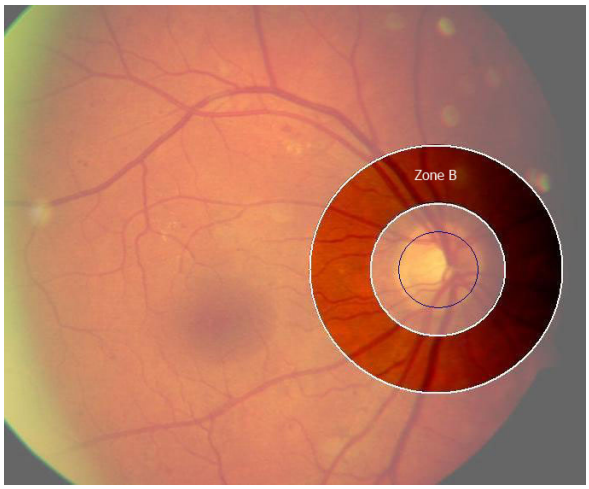

Fig. 2. Zone B in an experimental image. The zone has a diameter of 70 pixels surrounding the optic disk.

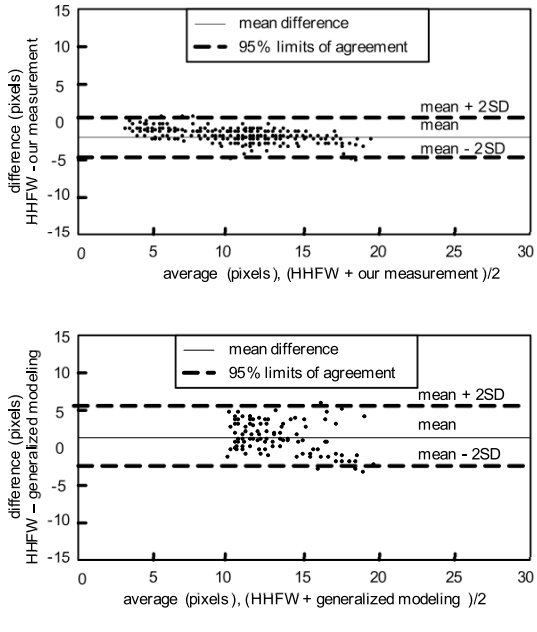

Fig. 3. Bland-Altman plot of width differences: (a) between the HHFW measurements and our measurements against the average of the two measurements; and (b) between the HHFW measurements and the generalised profile modelling measurements against the average of the two measurements.

IV. Discussion

We have presented a new approach of vessel detection on retinal images. The main contributions of this work are (i) to define a universal representation of vessel cross-sectional profiles in the Fourier domain, and (ii) to utilise phase congruency to characterise this representation. The proposed Fourier profile accommodates for upward and downward cross-sectional profiles with varying sharpness, and takes into account the vessel inner part which is blurred in some cases. Thanks to phase congruency our approach is invariant to brightness variations of the vessel.

A distinct advantage of the new approach is that it is effective even in the presence of thin and thick vessels. The algorithm is beneficial to detection and analysis in more advanced retinopathy where high-resolution retinal images are acquired. An important aspect of our approach is that it is effective with little operator intervention. This makes the algorithm attractive to detection and analysis on images of several types or image sequences. In contrast, existing methodologies are ineffective in the presence of a wide range of vessels, and may require choosing optimal parameter values or choosing a combination of predefined profile models. We conclude by stating that the new approach is promising for automated vessel detection where optimising profile models is difficult and preserving vessel width information is necessary.

References

[1] M. Gunn, "On ophthalmologic evidence of general arterial disease," *Transactions on Ophthalmology Society UK*, vol. 18, pp. 365–381, 1998.

[2] A. Frangi, W. Niessen, K. Vincken, M. Viergever, " Multiscale vessel enhancement filtering," in *Proc. 1998 MICCAI*, pp. 130-137.

[3] D. Farnell, F.N. Hatfield, P. Knox, M. Reakes,, S. Spencer, D. Parry, S.P. Harding, "Enhancement of Blood Vessels in Digital Fundus Photographs via the Application of Multiscale Line Operators," *Journal of the Franklin Institute*, vol. 345, pp. 748-765, 2008.

[4] J. Staal, M. Abramoff, M. Niemeijer, M. Viergever, B. van Ginneken, "Ridge-based Vessel Segmentation in Color Images of the Retina," IEEE Transactions on Medical Imaging, vol. 23, pp. 501-509, 2004.

[5] M. Sofka, C. Stewart, "Retinal vessel centerline extraction using multiscale matched filters, confidence and edge measure," *IEEE Trans Med Img,* vol. 25, pp. 1531-1546, 2006.

[6] O. Wink, W. Niessen, M. Viergever, "Multiscale vessel tracking," *IEEE Trans Med Img,* vol. 23, pp. 130-133, 2004.

[7] M. Poon, G. Hamarneh, G., R. Abugharbieh, "Live-Vessel: Extending Livewire for Simultaneous Extraction of Optimal Medial and Boundary Paths in Vascular Images," In *Proc. 2007 MICCAI*, vol. 4792, pp. 444-451. Springer, Berlin.

[8] P. Kovesi, "Invariant Image Features from Phase Congruency," *Videre: J. of Computer Vision Research*, vol. 1, pp. 1-26, 1999.

[9] T. Zhu, "Fourier cross-sectional profile for vessel detection on retinal images," *Comput Med Imaging Graph*, vol. 34, pp. 203-12, 2010.

[10] H. Li, W. Hsu, M.L. Lee , and H. Wang, "A piecewise Gaussian model for profiling and differentiating retinal vessels," In *Proc. 2003 IEEE Intl Conf Imag Proc*, pp.1069-1072.

[11] H. Narasimha-Iyer, V. Mahadevan, J.M. Beach, and B. Roysam, "Improved detection of the central reflex in retinal vessels using generalized dual Gaussian model and robust hypothesis testing," *IEEE Trans Inf Tech BioMed*, vol. 12(3), pp.406-410, 2008.